ACS APPLIED MATERIALS & INTERFACES

Research Article

www.acsami.org

Laser-Induced Graphene Layers and Electrodes Prevents Microbial Fouling and Exerts Antimicrobial Action

Swatantra P. Singh,[†] Yilun Li,[‡] Avraham Be'er,[†] Yoram Oren,[†] James M. Tour,*[,‡] and Christopher J. Arnusch*[,†]

[†]Department of Desalination and Water Treatment, Zuckerberg Institute for Water Research, The Jacob Blaustein Institutes for Desert Research, Ben-Gurion University of the Negev, Sede-Boqer Campus, 84990, Israel

[‡]Department of Chemistry, Department of Materials Science and NanoEngineering, Smalley-Curl Institute and NanoCarbon Center, Rice University, 6100 Main Street, Houston, Texas 77005, United States

Supporting Information

ABSTRACT: Prevention of fouling on surfaces is a major challenge that broadly impacts society. Water treatment technologies, hospital infrastructure, and seawater pipes exemplify surfaces that are susceptible to biofouling. Here we show that laser-induced graphene (LIG) printed on a polyimide film by irradiation with a CO_2 infrared laser under ambient conditions is extremely biofilm resistant while as an electrode is strongly antibacterial. We investigated the antibacterial activity of the LIG surface using LIG powder in suspension or deposited on surfaces, and its activity depended on the particle size and oxygen content. Remarkably, the antimicrobial effects of the surface were greatly amplified when voltages in the range of 1.1−2.5 were applied in an electrode configuration in bacterial solutions. The bactericidal mechanism was directly observed using microscopy and fast photography, which showed a rapid bacterial movement toward the LIG surface and subsequent bacterial killing. In addition, electrochemical generation of H_2O_2 was observed; however, the bacterial killing mechanism depended strongly on the physical and electrical contact of the bacterial cells to the surfaces. The anti-biofilm activity of the LIG surfaces and electrodes could lead to efficient protection of surfaces that are susceptible to biofouling in environmental applications by incorporating LIG onto the surfaces.

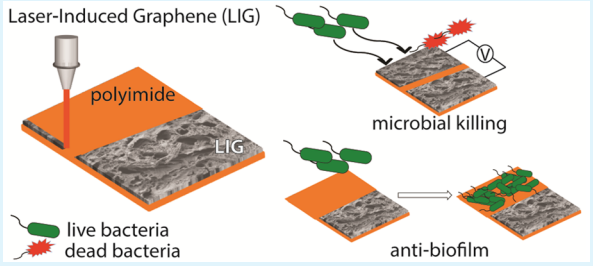

KEYWORDS: *graphene, laser-induced graphene, biofilm, antibacterial, electrodes*

INTRODUCTION

Graphene, a single atomic layer of sp^2-hybridized carbon atoms in a hexagonal crystal structure, has inimitable physical, chemical, electrical, and mechanical properties.[1,2] This exciting material has proven to be broadly applicable, from electronics to biotechnology, and has advanced, for example, solar cells, biomedical devices, and environmental technology.[3−6] Its material properties such as high surface area, conductivity, and mechanical strength make graphene an ideal candidate for environmental applications.[7] Graphene-based noble sorbents, electrocatalysts, photocatalysts, biosensors, antibacterial materials, and electrodes are envisioned to be the next-generation building blocks for technologies that remediate water and air pollution.[7]

In recent years, researchers have shown that graphene-based nanomaterials exhibit antibacterial properties.[8−10] Studies have demonstrated toxicity for Gram-positive, Gram-negative, phytopathogens, and also toward biofilm formation.[8−11] The nanosized sharp edges of graphene and its atomic composition are reported to contribute to its antibacterial properties,[10,12] with observations of cell wall puncturing and induction of bacterial oxidative stress.[8,12] However, the diversity of the chemical composition and structural form of the graphene material has given diverse observations. For example, Lie and co-workers have shown a higher toxicity of graphene oxide particles compared to reduced graphene oxides and concluded that a smaller size and a high functional-group density on graphene particles have more antibacterial activity.[13] Also, other graphene-based nanomaterials in the solution phase inhibited the growth of the bacteria but showed reduced cytotoxicity compared to graphene on surfaces.[7,8,10,12]

Environmental applications of graphene-based electrochemical sensors and electrodes were used in contaminant monitoring and removal, respectively,[7,14] and various other electrode materials have been used for electrochemical disinfection.[15−17] However, relatively high current densities and voltages are used to generate chlorine species. On the one hand, graphene's high surface area and remarkable intrinsic charge carrier mobility combined with antimicrobial properties might render this material a highly effective electrode with antimicrobial functionality.[7,18] Graphene doping and functionalization may further improve the efficacy of the electrodes; on

Received: April 6, 2017
Accepted: May 9, 2017
Published: May 18, 2017

DOI: 10.1021/acsami.7b04863
ACS Appl. Mater. Interfaces 2017, 9, 18238−18247

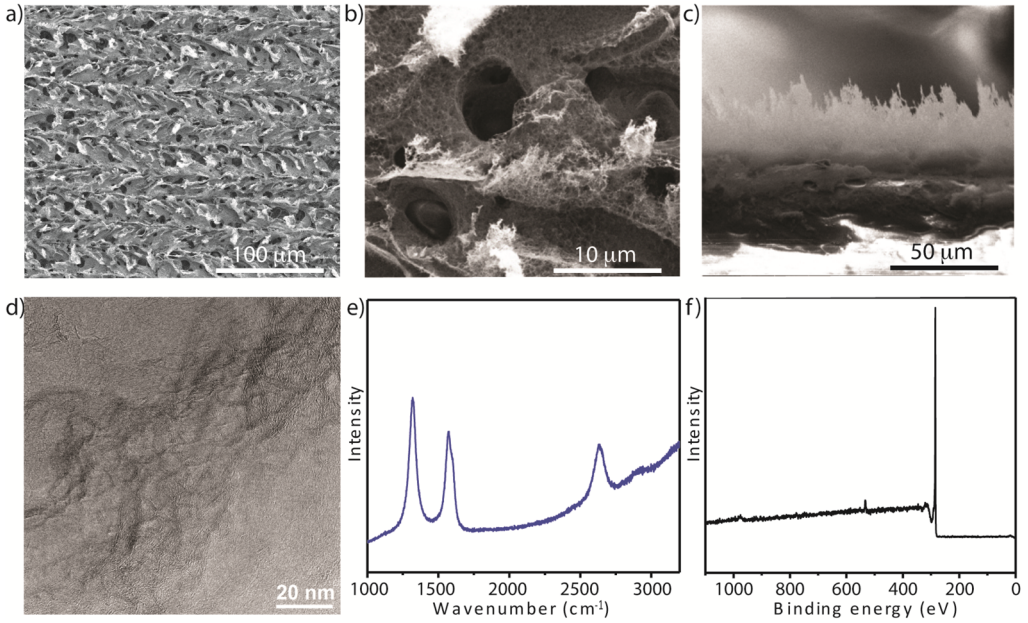

Figure 1. LIG fabricated on PI film using 2% laser power (75 W), in atmospheric conditions. (a, b) SEM top view images at different resolutions; (c) SEM cross-sectional image; (d) TEM image; (e) Raman spectrum; (f) XPS spectrum.

the other hand, such fabrication methods are very tedious and costly.[7,19] Recently, laser induction was found to be a robust and rapid method for preparing thin graphene layers on polyimide (PI) films, showing potential applications in energy storage devices such as supercapacitors.[19−21] In the present study, we evaluated the potential of the material to be used in environmental applications by investigating the antimicrobial and anti-biofilm properties of the laser-induced graphene (LIG) as fabricated on the PI surface or as electrodes. It was found that, when no external voltage was applied, LIG showed exceptional anti-biofouling properties. LIG's antimicrobial ability was greatly enhanced when stimulated by an external voltage. We then investigated mechanistic aspects of the bacterial killing process of the LIG by studying the antibacterial properties of LIG powders with different size distributions, either as applied on a membrane surface or in suspension. Remarkably, aspects of the LIG electrode-killing mechanism were revealed: We monitored the movement of the bacteria to the electrodes and killing in real time using fast epifluorescence microscopy. We observed different morphological changes of the bacteria using scanning electron microscopy (SEM) on the cathode in comparison to the anode and rationalized the relative contributions of indirect bacterial killing via chemical oxidative species to direct electrical effects. LIG could be widely applicable for the prevention of fouling on surfaces especially in water treatment technology.

RESULTS AND DISCUSSION

Synthesis and Characterization of LIG. Laser scribing of PI surfaces to produce LIG has been shown to be a cost-effective and efficient manner to pattern surfaces with graphene containing carbon nanomaterials.[19] The scribing was performed at atmospheric conditions using a 10.6 μm CO_2 laser at 2% of the laser power (75 W), and it resulted in a black conductive layer embedded on the PI film substrate. Imaging of the LIG surface using SEM revealed a highly porous foamlike structure with a cross-sectional thickness of ca. 20 μm (Figure 1a−c). We attributed the nanosized ripples seen in the transmission electron microscopy (TEM) images to exposed edges of the graphene layers (Figure 1d). This rippling structure might be due to the thermal expansion caused by the laser irradiation: The graphene formation by the laser was most likely a photothermal process, as a long-wavelength laser was used in the present study in combination with a relatively long pulse.[19] Laser-induced high localized temperatures (>2500 °C) can break the C−O, C═O, and C−N bonds of PI, and small molecules are released as gases, while the aromatic components can rearrange to form the graphene elements in the final composition.[19] Raman spectra (Figure 1e) showed characteristics of graphene and included a D peak at ∼1350 cm^{-1}, a G peak at ∼1580 cm^{-1}, and a 2D peak at ∼2700 cm^{-1}. The presence of the 2D peak supported the existence of the single-layer graphene sheets.[19,22] The X-ray photoelectron spectroscopy (XPS) spectrum (Figure 1f) of the LIG showed an elemental composition of mainly carbon (95.8%) and oxygen (4.2%). The X-ray diffraction (XRD) pattern of LIG showed peaks at 25.9° (2θ) for the 002 plane and a second peak at 42.9° (2θ), which corresponded to the 100 plane (Figure S3). The peak at 25.9° (2θ) gave an interlayer spacing of 3.4 Å and indicated a high level of graphitization, and the peak at 42.9° (2θ) was associated with an in-plane structure. We calculated the crystalline sizes along *c* axis (Lc) and domain size in the *a* axis (La) to be 1.6 and 5.8 nm using equations S1 and S2 (see Supporting Information), respectively. Taken together, the characterization confirmed that the fabricated samples were indeed LIG.[19]

LIG Resists Biofilm Formation. We studied the electrically conductive LIG as a single surface at open-circuit potential or as electrode pairs with an externally applied voltage. First, the antimicrobial activity of single surface LIG was investigated using *Pseudomonas aeruginosa*, a well-characterized species commonly used for biofilm research, in which the surfaces were subjected to biofilm growth conditions using a flow cell reactor. These were compared to unmodified PI surfaces as well as graphite surfaces (Figure 2). The LIG resisted the formation of biofilm growth without any other influence, and almost no

DOI: 10.1021/acsami.7b04863
ACS Appl. Mater. Interfaces 2017, 9, 18238−18247

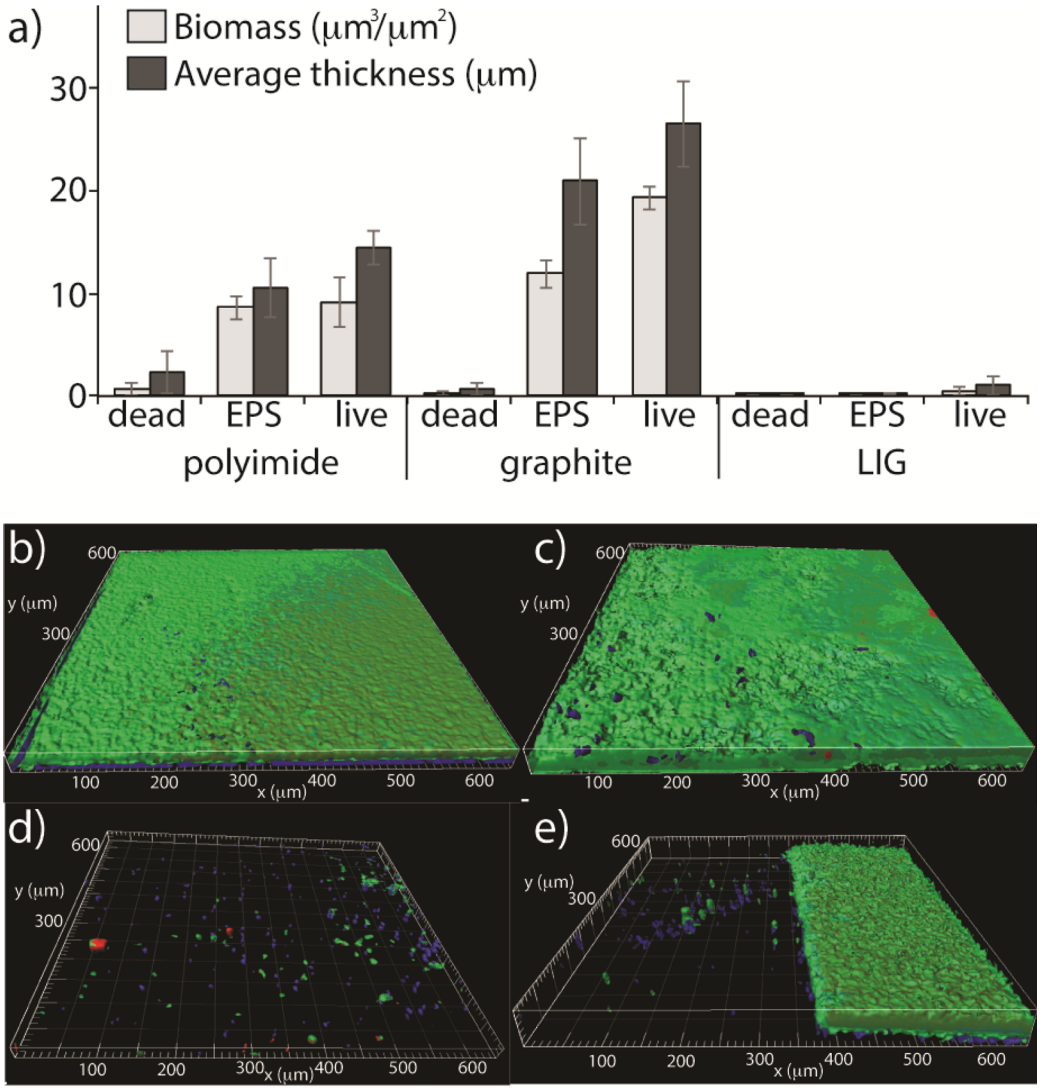

Figure 2. (a) Biofilm growth on the PI, graphite, and LIG surfaces with *P. aeruginosa* showing biomass and average thickness. Representative IMARIS software images for (b) PI; (c) graphite; (d) LIG; (e) the interface between the LIG (left) and PI film (right). Green represents live bacteria, red represents dead bacteria, and blue represents EPS.

biofilm was observed. In contrast, both PI and graphite controls showed large amounts of both live bacteria and extracellular polymeric substances (EPS) and less amounts of dead bacteria. The largest biovolume was observed on graphite up to a thickness of 26 μm. We identified dead bacteria under the biofilm near the surface of the PI and graphite materials using three-dimensional (3D) visualization of the biofilm with IMARIS-Bitplane software. This layer of dead bacteria suggested that the overlying thick layer of biofilm might have caused unfavorable growth conditions near the surface such as a lack of nutrients. LIG surfaces, however, showed extremely low amounts of adhered live bacteria, dead bacteria or EPS, and underlined the potential for use as antibiofilm surface coatings; a desirable feature for water and wastewater treatment technologies.[11] The stark contrast of biofilm growth between the LIG surface and the PI substrate was especially observed in images of the boundary regions between the materials (Figure 2e). We suggest two possible explanations for the absence of biofilm on LIG: First, the physical and chemical properties of the LIG surface might prevent bacterial adherence to the surface. The zeta potential of LIG at pH 7.4 was −44.4 mV, less negative than PI (−76.1 mV) and graphite paper (−117.6 mV; Figure S4). Since the zeta potential of *P. aeruginosa* PAO1 was reported to be ca. −23.3 mV at pH 7.4,[23] electrostatic repulsion of bacteria may initially play a role in inhibiting initial bacterial attachment on the negatively charged surfaces. However, highly negatively charged surfaces can be more quickly fouled with organic matter and thus be more susceptible to biofilm formation.[24] Biofilms were extensively seen on PI and graphite under these conditions, and this contrast to LIG surfaces could suggest that additional factors govern the phenomenon. The water wettability of LIG, PI, and graphite paper were determined and found to be significantly different. Contact angle analysis showed that LIG was the most hydrophilic (45.3° ± 3.8) compared to graphite (61.3° ± 6.6) and PI (74.5° ± 3.3; Figure S5). A more highly hydrophilic surface adsorbs significantly fewer hydrophobic components such as the hydrophobic components of EPS or dissolved organic matter from the solution, which can condition the surface for enhanced bacterial attachment.[25,26] In this case, electrostatic interactions masked under a conditioning layer would thus be less important in prevention of bacterial attachment and biofilm

DOI: 10.1021/acsami.7b04863
ACS Appl. Mater. Interfaces 2017, 9, 18238−18247

growth. We observed that EPS was not present on the LIG surfaces.

Second, the lack of biofilm could be due to the antimicrobial properties of graphene, which can contribute to an unfavorable environment for bacterial biofilm growth or direct bacterial toxicity. Various types of graphene have been reported to be antimicrobial;[7,8,13] thus, toxicity assays were performed using the LIG as fabricated on the PI surface and compared to LIG powders, made by scraping the LIG layer from the surface. The importance of these measurements lies in previous reports showing that graphene particle morphology, size, and oxygen content are factors contributing to bacterial toxicity.[8,10] Accordingly, we fabricated LIG powders with small and large particle size distributions by sonication of scraped LIG, which resulted in average particle sheet areas of 0.09 and 0.55 μm^2 using atomic force microscopy (AFM), respectively (Figure S6). A sample of the small-sized LIG powder was further oxidized using $KMnO_4$ as previously reported,[8,10] which increased the oxygen content of the LIG powder from 4% to 31% as measured using XPS (Figure S7). For the oxidized powder, deconvolution of the C 1s peak revealed that following the sp^2 C═C peak at 284.5 eV, O−C−O was most abundant at 286.8 eV, followed by C−OH and O═C−O at 285.2 and 288.5 eV, respectively (Figure S7d). The antibacterial efficacy of the LIG as made on the surface of PI was measured and compared to the LIG powders that were deposited on mixed cellulose filters (Figure 3). We observed a relatively minor

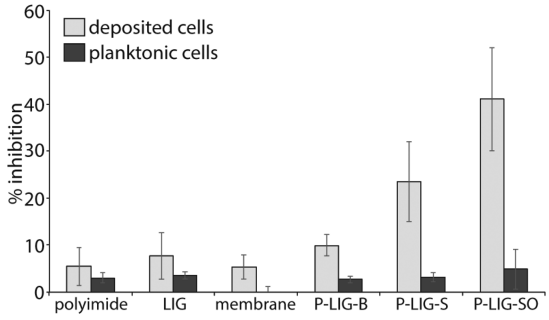

Figure 3. Inhibition of attached *P. aeruginosa* on PI, and LIG surfaces compared to mixed cellulose membrane surfaces with deposited LIG powder. Powder-LIG-big particles (P-LIG-B); Powder-LIG-small particles (P-LIG-S); Powder-LIG-small particles, oxidized (P-LIG-SO).

effect for the LIG surface, and the LIG powder with the large particle size distribution (average sheet size 0.55 μm^2) after 6 h of surface contact with a solution of *P. aeruginosa*. The sample with a smaller particle size distribution (0.09 μm^2) showed an increase in killing (~23%) of the attached cells, and the LIG powder with the small size that was oxidized was the most antimicrobial to attached cells (~41% killing), an observation similar to other reports.[13] The surfaces were not toxic to cells that did not directly contact the surface. The smaller particle size of graphene might be more toxic to bacteria as compared to larger particles due to the increased surface area and small edge features, while a higher oxygen content can lead to higher oxidative stress.[8,13] Thus, the morphology and low oxygen content of the presently fabricated LIG surface on PI films could have contributed to a relatively low antimicrobial property. Variable LIG fabrication conditions including laser power and synthesis atmosphere might affect the morphology of the LIG and its oxygen content; thus, antimicrobial activity might be enhanced on other types of LIG.

Next, we investigated the antimicrobial activity of the LIG powders in solution for their effect on planktonic bacteria (Figure 4). *P. aeruginosa* cell suspensions were exposed to 300

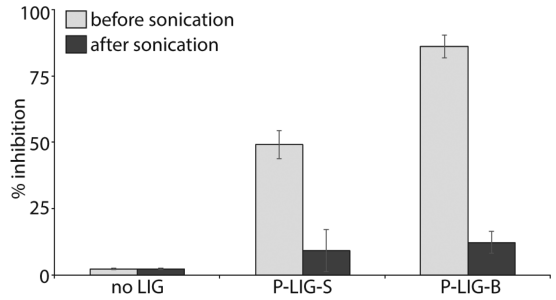

Figure 4. Comparison of the antibacterial action in using *P. aeruginosa* in solution with suspensions of powder-LIG-small (P-LIG-S) and of powder-LIG-big (P-LIG-B). A solution without any LIG was used as the control.

$\mu g/L$ of the LIG powders of different sizes for 6 h, and the bacterial viability was observed using the spread plate method. The experiments were performed with or without a sonication step before inoculation on the agar plate to release potentially viable bacteria from graphene aggregates. Indeed, in experiments performed without a sonication step, the LIG powder with a larger size distribution initially appeared to be more toxic compared to the sample with smaller particle sizes. However, when the experiment was performed with sonication of the sample before inoculation on the agar plate, the differences in antimicrobial activity were lost. This suggested that the LIG powders might have covered or entrapped the bacterial cells, which prevented their proliferation. The bacterial cells were not inactivated, but their growth was merely inhibited, similarly to the findings of Perreault et al.[8] Similar observations reported deactivated *Escherichia coli* cells after incubation for 24 h with graphene sheets, which could be subsequently reactivated by mild sonication.[27] We confirmed the antimicrobial activity by staining with Syto9/propidium iodide live/dead kit and imaging using confocal laser scanning microscopy (CLSM). Bacterial cells together with small or large LIG powder in suspension showed mostly live (green) bacteria (Figure S8). We observed aggregates when bacterial cells and LIG powder were mixed and suggest that entrapment of bacterial cells in LIG sheets is possible (Figure S8b,c).[8] Powder LIG deposited on mixed cellulose membrane surfaces showed both live and dead bacterial cells (Figure S9), and the powder LIG (small, oxidized) showed the highest antimicrobial activity (Figure S9d).

Antimicrobial Activity of LIG Electrodes. The antimicrobial activity of the LIG was dramatically increased when used as electrode pairs to which voltages in the range from 1.1 to 2.5 V were applied (Figure 5). The current voltage relationship for the graphene electrodes used in these experiments was recorded with 0.5 M NaCl solution (Figure S10). The electrodes were submerged in a solution containing ~1 × 10^4 or ~1 × 10^6 CFU mL^{-1} *P. aeruginosa*, and we observed that the highest voltage applied (2.5 V) was the most effective at eliminating viable bacteria from the solutions. More than 99% killing was observed within 4 h of operation (Figure 5a,c). Less activity was observed when 1.5 and 2.0 V were

DOI: 10.1021/acsami.7b04863
ACS Appl. Mater. Interfaces 2017, 9, 18238−18247

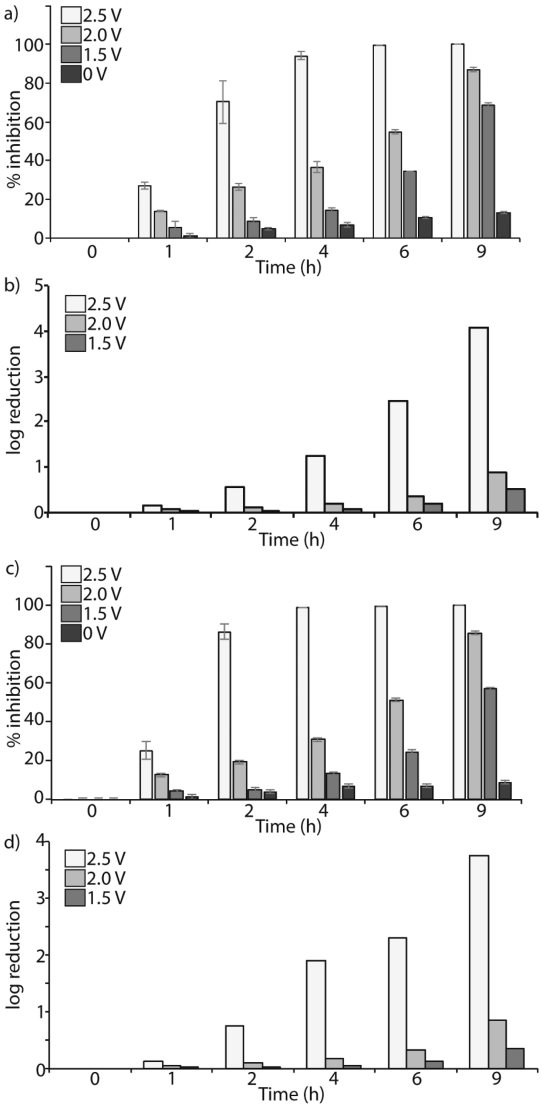

Figure 5. Inhibition of *P. aeruginosa* expressed as (a, c) % inhibition and (b, d) log reduction in the solution at different voltages (2.5, 2.0, and 1.5 V) with (a, b) low ~1 × 10^4 CFU mL^{-1} and (c, d) high ~1 × 10^6 CFU mL^{-1} bacteria loadings.

applied; however, an ~4 log reduction of bacteria was observed with these LIG electrodes with dilute bacterial solutions at 2.5 V. Similarly, an ~3.5 log reduction was observed in the concentrated bacterial solution (Figure 5b,d).

We investigated the mechanistic aspects of the bacterial killing process, which included possible chemical microbial toxicity, physical destruction due to contacting the LIG, or electrical effects of the graphene electrodes. First, the concentration of H_2O_2 was measured at each voltage in a pure solution of 0.05 M NaCl without bacteria (Figure 6). After 9 h of operation, only 0.3–0.9 mg L^{-1} H_2O_2 was measured. Active chlorine species (Cl_2 and $HOCl/^{-}OCl$) could not be detected: The formation of chlorine gas might have occurred but could have quickly reacted with H_2O_2, leading to the presence of the dominant species.[28] The H_2O_2 concentration was voltage-dependent and ranged from 0.3 to 0.7 after 6 h of operation in the experiment with the dilute bacterial solution (Figure S11). However, at all voltages measured, H_2O_2 was below the detection limit in the experiments using concentrated bacterial solution. The high amount of bacteria and associated

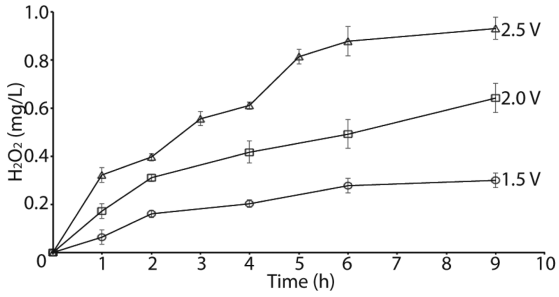

Figure 6. Generation of H_2O_2 by LIG electrodes at 1.5, 2.0, and 2.5 V measured in bulk solution.

organic matter most likely consumed the H_2O_2. To assess the contribution of H_2O_2 to the overall killing mechanism of the LIG electrodes, we tested the toxicity of 1 mg L^{-1} H_2O_2 exogenously added to *P. aeruginosa* cultures with LIG electrodes present at 0 V (open-circuit voltage). The viability was not affected in dilute or concentrated solutions of bacteria (Tables S1 and S2). However, in the case of H_2O_2 generation by the electrodes, the local concentration of H_2O_2 near the electrode surface would be much higher than the measured bulk concentrations, and H_2O_2 is continuously generated throughout the entire experiment.

We investigated the electrical effects using a special LIG electrode configured for use under the microscope (Figure S2). A 100 μm gap between the electrodes was designed so that both the cathode and anode could be observed simultaneously. A suspension of *P. aeruginosa* expressing green fluorescent protein (GFP_ was added to the top of the electrodes and was monitored as a function of time at different voltages (Figure 7). When no voltage was applied, the bacteria were unaffected and persisted in the solution. However, upon applying voltages above 1.1 V, bacterial movement toward the anode was observed, and subsequent disappearance of the cells was seen between 1.5 and 2.5 V (see video S1). At 1.1 V, no bacterial disappearance was seen after 30 s (Figure S12); however, the disappearance of bacteria was increasingly pronounced and correlated to the increase in voltage from 1.5 to 2.5 V. For example, at 1.5 V, bacteria began to disappear at the anode side after 1 s, and the bacteria also began to disappear from the cathode side after 2 s, with almost complete disappearance of the bacteria at 30 s. Faster disappearance of bacterial cells was seen at higher voltages 2.0 and 2.5 V, where almost complete disappearance of the bacteria was observed after 1 s (Figure 7e–h and 7i–l).

The movement of bacteria toward the LIG surfaces and their subsequent disappearance indicate that the electrical effect, in combination with a surface toxicity effect and localized active chemical species generation, is the most plausible explanation for the mode of antibacterial action of the LIG electrodes. *P. aeruginosa* cells have a negative surface charge due to negatively charged biomolecules present in the cell membrane such as phospholipids and polysaccharides,[29] and this could be attracted toward the anode. The attraction of the bacteria toward the anode could also expose them to higher concentrations of active chemical species, since the concentrations are significantly higher at the surface of the electrode than in the bulk solution.[23] Moreover, the toxicity of the graphene morphology at the surface might be greatly enhanced if the bacterial cells are forced to contact due to the electric field. The effect of electric potential on microorganisms has

DOI: 10.1021/acsami.7b04863
ACS Appl. Mater. Interfaces 2017, 9, 18238–18247

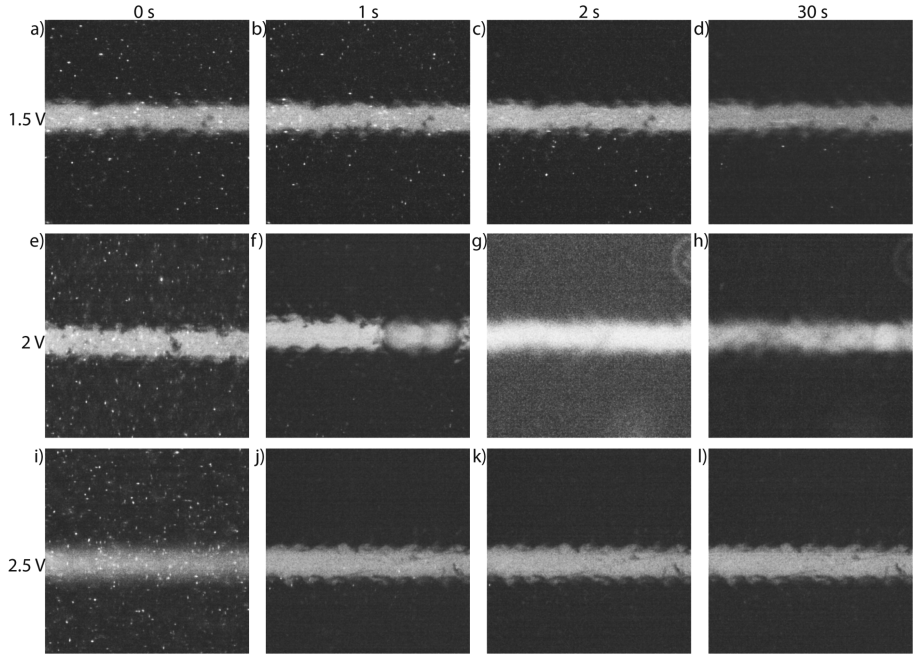

Figure 7. GFP-tagged *P. aeruginosa* were observed using epifluorescence microscopy on electrodes made of LIG. Voltages (1.5−2.5 V) were applied and images were captured up to 30 s. In each image, the anode (top) was separated from the cathode (bottom) by a 100 μm channel. GFP tagged *P. aeruginosa* were observed as bright dots (see also Movie, Supporting Information).

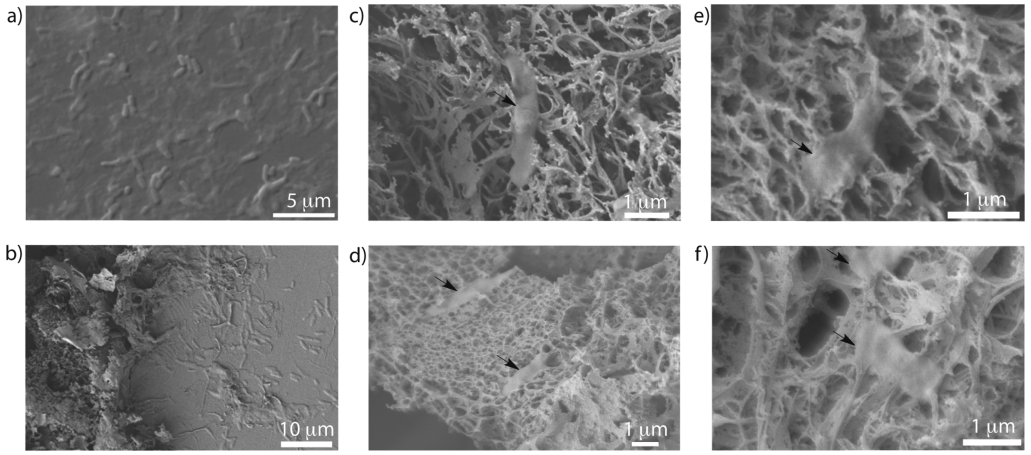

Figure 8. *P. aeruginosa* was visualized on LIG electrodes using SEM after application of 1.5 V for 30 s. (a) Bacteria at a PI surface (without electricity). (b) Bacterial cells seen in the PI channel between the LIG electrodes. (c, d) Damaged bacterial cells (elongation) at anode. (e, f) Damaged bacterial cells at the cathode; arrows indicate bacteria.

been discussed in the literature,[25,30−32] and physical bacterial damage from the electric current can occur from irreversible electroporation or direct electron transfer, for example.[31−33] Also, a fast denaturation of proteins in the presence of an electric field can lead to toxic effects on the bacteria;[34] however, in the present study the instantaneous destruction of the cells suggests a rapid physical destruction of the cell wall or cell membrane components. The high surface area of the LIG electrode (103 m^2/g) can lead to high currents and can enhance the electrochemical processes at low voltages (1.5 to 2.5 V), which contributes to higher decontamination rates by the LIG electrodes. Compared to graphite electrodes configured in the same way, the movement of bacterial cells began only at 2.3 V, and disappearance of bacteria was observed only above 2.6 V. The graphite electrodes showed relatively lower currents compared to the LIG electrodes and might have contributed to their lower activity (Table S3).

To visualize the possible destructive effects of the LIG electrode surfaces on bacteria, and to characterize changes in the cell morphologies at the cathode and anode, SEM images were obtained of the fixed bacteria after an applied voltage of 1.5 V for 30 s (Figure 8). Bacteria were mainly seen on the PI parts of the electrode, including the channel between the electrodes (Figure 8a,b). In general, only a small number of bacteria on the LIG could be identified on the electrodes and could suggest a rapid disintegration of the cells, and this underlines the antifouling ability of the LIG electrode surface. Of the bacteria observed on the surfaces, an increase in the cell length was seen at the anode (Figure 8c,d), as compared to bacteria on the cathode (Figure 8e,f) or without electricity (Figure 8a). Since a movement of cells was observed toward the

DOI: 10.1021/acsami.7b04863
ACS Appl. Mater. Interfaces 2017, 9, 18238−18247

anode under the electric field, the deformation and elongation of the cells can occur as they are pulled against the rough anode surface. At the cathode, burst cells were seen (Figure 8e,f), probably due to contact with the graphene, damage from the in situ generation of cathodic H_2O_2, and a possible irreversible electroporation processes. Compared to the batch decontamination experiments, the bacterial killing process in the microscopy electrode configuration occurred much faster. This can be due to differences in electrode configuration, flow conditions, and current density.[35] For example, the bacterial cells in the microscope study were applied very close to the electrodes in contrast to the batch experiments, where bacteria are present mainly in the bulk solution.

We tested the applicability of the material for environmental applications by using secondary treated wastewater that consisted of a complex mixture of natural organic matter, colloidal material, salts, and microbes, including both Gram-positive and Gram-negative bacteria. We recently reported the bacterial community analysis of the microbes from this water that had adhered to membrane surfaces, and the five most abundant bacterial phyla identified included Actinobacteria, Bacteroidetes, Firmicutes, Proteobacteria, and candidate phylum TM6.[36] Thus, we tested the LIG electrodes in solutions containing 10% wastewater and wastewater adjusted to $\sim 1 \times 10^4$ and $\sim 1 \times 10^6$ CFU/mL. In all cases greater than 99.9% bacterial inhibition was observed after 9 h of operation at a voltage of 2.5 V (Figure S13). Moreover, a strong anti-biofilm effect was observed (Figure S14) and shows the utility of the LIG surfaces and electrodes in these complex wastewater solutions.

CONCLUSION

The antimicrobial and anti-biofilm properties of LIG underline the importance of the material especially for environmental applications where biofilm and microbial growth is undesirable. The rapid generation of LIG combined with the versatility of directly printing this material on PI surfaces can enable this material to be quickly applied in new technologies as anti-biofouling surfaces and electrodes.

MATERIALS AND METHODS

General. PI (Kapton) film with thickness 127 μm (catalog No. 2271K6) was purchased from McMaster-Carr, USA. Graphite sheets (PAPYEX-SR) were obtained from Merson, Germany. Sodium chloride (NaCl, 99%), sodium phosphate dibasic heptahydrate ($Na_2HPO_4{\cdot}7H_2O$ > 99%), and monobasic potassium phosphate (KH_2PO_4, 99%) were obtained from Merck, Israel. Hydrogen peroxide (H_2O_2, 30%) was obtained from J. T. Baker. Ethanol (anhydrous 99.5%) was obtained from Macron fine chemicals. Glutaraldehyde solution (50%) and paraformaldehyde (95%) were purchased form Sigma-Aldrich, Israel. LIVE/DEAD BacLight bacterial viability kit, containing propidium iodide and SYTO 9, and H_2O_2/Peroxidase Assay Kit (Amplex Red) were obtained from Thermo Fisher Scientific (Molecular Probes, USA). DPD chlorine kit (AQUANAL), and 2,9-dimethyl-1,10-phenanthroline (neocuproine, ~98%) were purchased from Sigma-Aldrich, Israel. Unless specified, all chemicals were dissolved in deionized (DI) water obtained from a Milli-Q ultrapure water purification system (Millipore, Billerica, MA). The DC power supply was model Le305D (Lion, 0−30 V 5A).

Fabrication and Characterization of LIG. Laser induction was conducted on a PI film substrate with an XLS10MWH (Universal Laser Systems) laser platform, equipped with a 10.6 μm CO_2 pulsed laser (75 W). An image density of 1000 pulses per inch in both axis and a rastering speed of 30 cm/s were used for all experiments. A nozzle provided with the instrument was used to blow air toward the laser spot, while the general atmosphere within the laser platform was still air at ambient pressure. A laser duty cycle of 2% was used to prepare the LIG samples. SEM images were taken with an FEI Quanta 400 ESEM. TEM characterizations were performed using a 200 kV JEOL 2100 Field Emission Gun TEM. Raman spectra were recorded with a Renishaw Raman RE01 scope with 633 nm laser. XPS was performed on a PHI Quantera SXM scanning X-ray microprobe with 200 μm beam size and 45° takeoff angle, and calibrated using C 1s at 284.5 eV. XRD was conducted on a Rigaku D/Max ultima II with Cu Kα radiation (λ = 1.54 Å). The surface area of LIG was measured with a Quantachrome autosorb-3b BET surface analyzer.

LIG Powder Preparation. LIG powder was made by scraping the LIG from the PI surface. Different LIG powder size distributions were obtained by probe sonication of scraped LIG, as previously described.[8,37] Briefly, a stable suspension of LIG powder (2.0 mg mL^{-1} in DI water) was made by immersion in a bath sonicator (D-74224, Elma Singen) for 30 min. This suspension was then probe-sonicated in an ice bath for 120 min at high intensity (VCX130, Sonics Vibra-cell) for smaller size distributions. After 120 min of probe sonication, 50 mL of the suspension was centrifuged at 12 000 × g for 30 min and then oxidized as previously described as follows.[8] LIG powder (100 mg) was placed in 5 mL of concentrated H_2SO_4. Then, $KMnO_4$ (0.75 g) was slowly added in an ice bath. The solution was heated to 35 °C for 2.5 h, and subsequently DI water (10 mL) was slowly added to the suspension. After 2 h, DI water (30 mL) and H_2O_2 (30%, 5.5 mL) were slowly added to the suspension. The solution was kept for 2 d at room temperature, and the precipitate was collected by centrifugation (12 000 × g, 30 min) and washed with HCl (10% vol, 3×) and DI water (3×) to remove chemical residues. Different types of prepared LIG powder were deposited on a membrane surface (mixed cellulose esters, 0.025 μm, MF-Millipore Membrane Filter) by filtering a suspension of 5 mL (2.0 mg L^{-1} in DI) onto the membrane filter followed by air drying. LIG powders were characterized using Raman spectroscopy (LabRam HR with 633 nm laser), XPS (ESCALAB 250 Thermo Fisher Scientific), and SEM (JSM-7400F, JEOL). AFM images were captured by Cypher-ES (Asylum Research/Oxford Instruments) with a AC160TS (Olympus, resonance frequency of 300 kHz).

Bacteria Preparation. *P. aeruginosa* (PAO1) wild type and GFP-tagged cultures, bacterial strains commonly used for biofilm research and well-characterized,[11] were grown in Luria−Bertani (LB) broth at 30 °C and harvested in mid-exponential phase, which was verified by measuring the optical density at 600 nm. Cultures were centrifuged at 4000 rpm for 15 min, and cells were washed three times with 0.9% saline solution to remove residual medium constituents. The bacterial cells were further diluted to $\sim 1 \times 10^8$ colony-forming units (CFU) mL^{-1} in 0.9% saline solution for the experiments. GFP-tagged *P. aeruginosa* (PAO1) was used for the LIG electrode experiments. Real-time observation of GFP-tagged PAO1 was done under the fluorescent microscope. Secondary treated wastewater was gathered from an aeration pond located at Kibbutz Sde Boker (Israel). The water contained $(1.6 \pm 0.2) \times 10^4$ CFU mL^{-1}, determined using the spread plate method on LB agar media and followed by incubation for 24 h at 30 °C. Secondary treated wastewater (1 mL) was added to 50 mL of LB broth and prepared as above.

Biofilm Growth Experiments. *P. aeruginosa* cultures (wild type) or mixed wastewater bacterial cultures were grown in LB until midexponential phase. Cells were harvested and washed with LB broth and diluted to an OD of 0.1 at 600 nm in LB broth. Anti-biofilm experiments were performed in a custom-made flow cell device as reported before.[24] The LIG-coated PI samples, a graphite sample, and an untreated PI film were attached to a glass slide with double-sided tape and vertically placed in the flow cell. The biofilm experiment consisted of inoculation of the surfaces with *P. aeruginosa* by flowing 50 mL of bacterial suspension through the flow cell at a rate of 2.5 mL min^{-1}, followed by flowing a nutrient media (10% LB) at 2.0 mL min^{-1} for 36 h. SYTO 9, propidium iodide, and concanavalin A conjugated to Alexa Fluor 633 dyes (ConA) were used for live, dead, and extracellular polymeric substances (EPS), respectively. Propidium iodide (1.5 μL, 20 mM) and SYTO 9 (1.5 μL, 3.34 mM) were added

DOI: 10.1021/acsami.7b04863
ACS Appl. Mater. Interfaces 2017, 9, 18238−18247

to 0.997 mL of 150 mM sodium chloride for staining dead and live bacteria, respectively. ConA-Alexa Fluor 633 (50 μL mL^{-1}) was prepared by dilution of the 5 mg mL^{-1} stock solution in 150 mM sodium chloride. Surfaces were carefully dried by paper tissue (Kimwipe) to remove excess electrolyte, and then 100 μL of the staining solutions were added to cover the biofilm surface and stored protected from light for 20 min. The surfaces were gently washed (3×) by adding 0.25 mL of sodium chloride solution (150 mM) to the surface and then carefully removing excess electrolyte by touching the edges with absorbing paper. Evaluation of the biofilm was done by CLSM (Zeiss LSM 510, META), with Zeiss dry objective plan-NeoFluar (20× magnification and numerical aperture of 0.5), as previously described.[38,39] An excitation wavelength of 488 nm was used for both the SYTO 9 and the PI, and 633 nm was used for the Alexa Fluor 633. Biofilm images were prepared by Imaris 3D imaging software (Bitplane, Zurich, Switzerland), and quantitative analysis (biofilm volume and average thickness) was calculated using COMSTAT on Matlab 2015b.[40]

Surface Antimicrobial Activity. The antibacterial activity of the materials was measured using intact LIG-coated surfaces (1 cm^2) or surfaces with deposited LIG powder using a recently reported method.[8] Briefly, 1 mL of diluted *P. aeruginosa* (PAO1) wild type (~1 × 10^6 CFU mL^{-1}) in saline solution was placed slowly on LIG modified membrane surface (~1 cm^2), and LIG films (~1 cm^2) and incubated at 30 °C in incubator for 10 min or 6 h. Then the membrane filters or LIG films were washed with 0.9% NaCl suspension to remove unattached bacterial cells. Subsequently, the surfaces were placed in 50 mL Falcon tubes containing 10 mL of 0.9% saline solution, and they were then bath-sonicated (Transonic Digitals, Elma, 20% power) for 10 min. Viable bacteria were assessed using the spread plate method on LB agar media and followed by incubation for 24 h at 30 °C before CFU enumeration. The results for the samples incubated for 6 h were compared to the respective samples that were incubated for 10 min. LIVE/DEAD fluorescent staining assays were used to visualize live and dead bacteria under an epifluorescence microscope. The surfaces were first stained with 3.34 μM SYTO 9 and 20 μM propidium iodide in 0.9% saline solutions[8] and were protected from light for 30 min. Samples were washed with 0.9% NaCl and analyzed using CLSM (20× and 40×) with 0.5 and 0.8 numerical aperture, respectively.

Solution Antimicrobial Activity. Reported methods were adopted as follows.[8,12] LIG powder (2.0 mg mL^{-1}) prepared as above was added to *P. aeruginosa* (1 × 10^6 CFU mL^{-1}) in 0.9% NaCl solution for a final concentration of 300 μg mL^{-1} and incubated for 6 h at room temperature with constant agitation. The cell suspensions were bath-sonicated and immediately spread on an agar media plate. CFU enumeration was performed after incubation at 24 h at 30 °C. LIVE/DEAD fluorescent staining was performed with 3.34 μM SYTO 9 (1.5 μL) and 20 μM propidium iodide (1.5 μL) in 997 μL of 0.9% saline bacterial solutions, and the bacteria were viewed using CLSM.

LIG Electrodes Antimicrobial Activity. A perforated PI sheet 10 cm × 7 cm was fabricated by laser-cutting square holes (4 mm × 4 mm) separated by 3 mm in a grid pattern. LIG (1 mm wide, 2% Laser Power 75 W) was printed on both sides of the PI sheet between the square holes for a total electrode surface area of 20 cm^2. Copper wires were connected to each electrode using a carbon-based glue and connected to the DC power supply. The electrode sheet was suspended in a beaker containing an aqueous solution of NaCl (1 L, 0.05 M; see Figure S1 Supporting Information). *P. aeruginosa* cells (1 × 10^8 CFU mL^{-1}) in 0.9% NaCl solution was prepared as described above and added to the beaker for a final concentration of ~1 × 10^4 CFU mL^{-1} (low loading) and ~1 × 10^6 CFU mL^{-1} (high loading) with constant stirring at room temperature. The power was adjusted to 0, 1.5, 2.0, or 2.5 V, and 1 mL samples were withdrawn from the reactor and used for CFU enumeration or H_2O_2/active chlorine species determination. Additionally, at 0 V, the experiment was performed with or without exogenously added H_2O_2 for an initial concentration of 1.0 mg L^{-1} of H_2O_2 in 0.05 M NaCl solution. H_2O_2 concentration was measured by H_2O_2/peroxidase assay kit (Amplex Red, Thermo Fisher) and copper(II) ion and 2,9-dimethyl-1,10-phenanthroline (DMP) method.[28] Active chlorine species was examined by the *N*,*N*-diethyl-*p*-phenylenediamine (DPD) method.[28] This experiment was also performed using 2.5 V with 10% secondary treated wastewater that was diluted with dechlorinated tap water or wastewater cultures that were adjusted to ~1 × 10^4 CFU mL^{-1} (low loading) and ~1 × 10^6 CFU mL^{-1} (high loading) as above.

Visualization of LIG Killing Action Using Fluorescence Microscopy. Two LIG electrode layers (1 × 0.4 cm each) separated by a 0.1 mm gap were fabricated by printing LIG (2% Laser Power 75 W) on a PI sheet as described above. Graphite threads were connected to each electrode using a carbon-based conductive glue and connected to the DC power supply (see Figure S2 Supporting Information). Connections were protected by transparent epoxy glue to avoid any interference. The two-electrode sheet was affixed on a microscope slide, and 5.0 μL of GFP-tagged *P. aeruginosa* suspension (~1 × 10^6 CFU mL^{-1}) in 0.9% NaCl solution was placed on the electrodes and covered with a glass coverslip. The bacterial cells were observed using optical microscopy (Zeiss Axio Imager Z2), equipped with a sensitive high-resolution video camera (NEO, Andor), to capture the motion under fluorescence microscopy (30 f/s and 1800 × 1800 pixels). No photobleaching was observed during acquisition times. We used a modified version for the filters and dichroic mirror. The GFP-labeled cells were observed by standard *yellow* fluorescent protein Zeiss illumination setup instead of the standard GFP one (filter set 46 yellow fluorescent protein shift free: excitation 500/25; beam splitter 515; emission 535/30). The voltage was varied between 0.0 and 2.5 V.

SEM. Surfaces were washed with 0.9% sterile saline solution and fixed with 2% paraformaldehyde and 2.5% glutaraldehyde in 0.2 M Sorenson's buffer (pH 7.2) and stored for 3 h. The samples were carefully dehydrated by immersion in a series of water/ethanol solutions (50, 70, 80, 90, and 100% ethanol). Samples were stored in a desiccator overnight at room temperature. Gold sputter coating was performed, and the samples were imaged using SEM (JSM-7400F, JEOL).

Zeta Potential. Electrokinetic Analyzer (SurPASS, Anton Paar Gmbh) was used for the evaluation of the zeta potential of the solid surfaces. Two identical samples of PI, LIG and graphite paper (2 cm × 1 cm), were used for the measurements. KCl (0.1 mM) was used as an electrolyte, and 0.1 N NaOH and 0.1 N HCl solutions were used to control the pH.

Contact Angle. The contact angle (θ) was measured by the captive bubble method with OCA-15 contact angle analyzer (DataPhysics, Filterstadt, Germany). Samples were taped to a glass coverslip and soaked in Milli-Q water prior to measurement. They were placed in the sample holder with the surface side facing down in Milli-Q water. An air bubble, 7 ± 3 μL, was injected under the sample surface, and the images were analyzed using the SCA 2.0 software.

■ ASSOCIATED CONTENT

Supporting Information

The Supporting Information is available free of charge on the ACS Publications website at DOI: 10.1021/acsami.7b04863.

Schematic apparatus setup, XRD, zeta potential, contact angle, AFM, XPS, epifluorescence microscopy images, current−voltage relationships and H_2O_2 generation of LIG electrodes, bacterial susceptibility to H_2O_2, testing of LIG with wastewater (PDF)

Movie of the bacterial response to LIG electrodes with applied voltage (MPG)

■ AUTHOR INFORMATION

Corresponding Authors

*E-mail: arnusch@bgu.ac.il. (C.J.A.)

*E-mail: tour@rice.edu. (J.M.T.)

ORCID

Yilun Li: 0000-0002-0750-2228

DOI: 10.1021/acsami.7b04863
ACS Appl. Mater. Interfaces 2017, 9, 18238−18247

James M. Tour: 0000-0002-8479-9328
Christopher J. Arnusch: 0000-0002-1462-1081

Notes

The authors declare no competing financial interest.

■ ACKNOWLEDGMENTS

We are grateful to the United States−Israel Binational Science Foundation (BSF Grant No. 2014233) for financial support. C.J.A. wishes to thank the Canadian Associates of Ben Gurion Univ. of the Negev (CABGU) Quebec Region for support. A.B. is thankful for partial support from The Israel Science Foundation Grant No. 373/16. The work at Rice Univ. was funded by the AFOSR (FA-9550-14-1-0111). We thank J. Hillman and Universal Laser Systems for providing the laser writing tool.

■ REFERENCES

(1) Geim, A. K.; Novoselov, K. S. The Rise of Graphene. *Nat. Mater.* **2007**, *6*, 183−191.
(2) Novoselov, K. S.; Geim, A. K.; Morozov, S. V.; Jiang, D.; Zhang, Y.; Dubonos, S. V.; Grigorieva, I. V.; Firsov, A. A. Electric Field Effect in Atomically Thin Carbon Films. *Science* **2004**, *306*, 666−669.
(3) Bitounis, D.; Ali-Boucetta, H.; Hong, B. H.; Min, D.-H.; Kostarelos, K. Prospects and Challenges of Graphene in Biomedical Applications. *Adv. Mater.* **2013**, *25*, 2258−2268.
(4) Choi, B. G.; Park, H.; Park, T. J.; Yang, M. H.; Kim, J. S.; Jang, S.-Y.; Heo, N. S.; Lee, S. Y.; Kong, J.; Hong, W. H. Solution Chemistry of Self-Assembled Graphene Nanohybrids for High-Performance Flexible Biosensors. *ACS Nano* **2010**, *4*, 2910−2918.
(5) Mohanty, N.; Berry, V. Graphene-Based Single-Bacterium Resolution Biodevice and DNA Transistor: Interfacing Graphene Derivatives with Nanoscale and Microscale Biocomponents. *Nano Lett.* **2008**, *8*, 4469−4476.
(6) Sun, Y.; Wu, Q.; Shi, G. Graphene Based New Energy Materials. *Energy Environ. Sci.* **2011**, *4*, 1113−1132.
(7) Perreault, F.; Fonseca de Faria, A.; Elimelech, M. Environmental Applications of Graphene-Based Nanomaterials. *Chem. Soc. Rev.* **2015**, *44*, 5861−5896.
(8) Perreault, F.; De Faria, A. F.; Nejati, S.; Elimelech, M. Antimicrobial Properties of Graphene Oxide Nanosheets: Why Size Matters. *ACS Nano* **2015**, *9*, 7226−7236.
(9) Chen, J.; Peng, H.; Wang, X.; Shao, F.; Yuan, Z.; Han, H. Graphene Oxide Exhibits Broad-Spectrum Antimicrobial Activity against Bacterial Phytopathogens and Fungal Conidia by Intertwining and Membrane Perturbation. *Nanoscale* **2014**, *6*, 1879−1889.
(10) Hu, W.; Peng, C.; Luo, W.; Lv, M.; Li, X.; Li, D.; Huang, Q.; Fan, C. Graphene-Based Antibacterial Paper. *ACS Nano* **2010**, *4*, 4317−4323.
(11) Yin, S.; Goldovsky, Y.; Herzberg, M.; Liu, L.; Sun, H.; Zhang, Y.; Meng, F.; Cao, X.; Sun, D. D.; Chen, H.; Kushmaro, A.; Chen, X. Functional Free-Standing Graphene Honeycomb Films. *Adv. Funct. Mater.* **2013**, *23*, 2972−2978.
(12) Akhavan, O.; Ghaderi, E. Toxicity of Graphene and Graphene Oxide Nanowalls against Bacteria. *ACS Nano* **2010**, *4*, 5731−5736.
(13) Liu, S.; Zeng, T. H.; Hofmann, M.; Burcombe, E.; Wei, J.; Jiang, R.; Kong, J.; Chen, Y. Antibacterial Activity of Graphite, Graphite Oxide, Graphene Oxide, and Reduced Graphene Oxide: Membrane and Oxidative Stress. *ACS Nano* **2011**, *5*, 6971−6980.
(14) Wang, Y.; El-Deen, A. G.; Li, P.; Oh, B. H. L.; Guo, Z.; Khin, M. M.; Vikhe, Y. S.; Wang, J.; Hu, R. G.; Boom, R. M.; Kline, K. A.; Becker, D. L.; Duan, H.; Chan-Park, M. B. High-Performance Capacitive Deionization Disinfection of Water with Graphene Oxide-Graft-Quaternized Chitosan Nanohybrid Electrode Coating. *ACS Nano* **2015**, *9*, 10142−10157.
(15) Brillas, E.; Martínez-Huitle, C. A. Decontamination of Wastewaters Containing Synthetic Organic Dyes by Electrochemical Methods. An Updated Review. *Appl. Catal., B* **2015**, *166*, 603−643.
(16) Martínez-Huitle, C. A.; Brillas, E. Decontamination of Wastewaters Containing Synthetic Organic Dyes by Electrochemical Methods: A General Review. *Appl. Catal., B* **2009**, *87*, 105−145.
(17) Feng, C.; Suzuki, K.; Zhao, S.; Sugiura, N.; Shimada, S.; Maekawa, T. Water Disinfection by Electrochemical Treatment. *Bioresour. Technol.* **2004**, *94*, 21−25.
(18) Tang, L.; Wang, Y.; Li, Y.; Feng, H.; Lu, J.; Li, J. Preparation, Structure, and Electrochemical Properties of Reduced Graphene Sheet Films. *Adv. Funct. Mater.* **2009**, *19*, 2782−2789.
(19) Lin, J.; Peng, Z.; Liu, Y.; Ruiz-Zepeda, F.; Ye, R.; Samuel, E. L. G.; Yacaman, M. J.; Yakobson, B. I.; Tour, J. M. Laser-Induced Porous Graphene Films from Commercial Polymers. *Nat. Commun.* **2014**, *5*, 5714.
(20) Li, L.; Zhang, J.; Peng, Z.; Li, Y.; Gao, C.; Ji, Y.; Ye, R.; Kim, N. D.; Zhong, Q.; Yang, Y.; Fei, H.; Ruan, G.; Tour, J. M. High-Performance Pseudocapacitive Microsupercapacitors from Laser-Induced Graphene. *Adv. Mater.* **2016**, *28*, 838−845.
(21) Peng, Z.; Ye, R.; Mann, J. A.; Zakhidov, D.; Li, Y.; Smalley, P. R.; Lin, J.; Tour, J. M. Flexible Boron-Doped Laser-Induced Graphene Microsupercapacitors. *ACS Nano* **2015**, *9*, 5868−5875.
(22) Ferrari, A. C.; Meyer, J. C.; Scardaci, V.; Casiraghi, C.; Lazzeri, M.; Mauri, F.; Piscanec, S.; Jiang, D.; Novoselov, K. S.; Roth, S.; Geim, A. K. Raman Spectrum of Graphene and Graphene Layers. *Phys. Rev. Lett.* **2006**, *97*, 187401.
(23) Liu, W. K.; Brown, M. R.; Elliott, T. S. Mechanisms of the Bactericidal Activity of Low Amperage Electric Current (DC). *J. Antimicrob. Chemother.* **1997**, *39*, 687−695.
(24) Bernstein, R.; Freger, V.; Lee, J.-H.; Kim, Y.-G.; Lee, J.; Herzberg, M. Should I Stay or Should I Go?" Bacterial Attachment *vs* Biofilm Formation on Surface-Modified Membranes. *Biofouling* **2014**, *30*, 367−376.
(25) Al-Juboori, R. A.; Yusaf, T. Biofouling in RO System: Mechanisms, Monitoring and Controlling. *Desalination* **2012**, *302*, 1−23.
(26) Haas, R.; Gutman, J.; Wardrip, N. C.; Kawahara, K.; Uhl, W.; Herzberg, M.; Arnusch, C. J. Glycosphingolipids Enhance Bacterial Attachment and Fouling of Nanofiltration Membranes. *Environ. Sci. Technol. Lett.* **2015**, *2*, 43−47.
(27) Akhavan, O.; Ghaderi, E.; Esfandiar, A. Wrapping Bacteria by Graphene Nanosheets for Isolation from Environment, Reactivation by Sonication, and Inactivation by Near-Infrared Irradiation. *J. Phys. Chem. B* **2011**, *115*, 6279−6288.
(28) Kosaka, K.; Yamada, H.; Matsui, S.; Echigo, S.; Shishida, K. Comparison among the Methods for Hydrogen Peroxide Measurements To Evaluate Advanced Oxidation Processes: Application of a Spectrophotometric Method Using Copper(II) Ion and 2,9-Dimethyl-1,10-Phenanthroline. *Environ. Sci. Technol.* **1998**, *32*, 3821−3834.
(29) Shephard, J.; McQuillan, A. J.; Bremer, P. J. Mechanisms of Cation Exchange by Pseudomonas Aeruginosa PAO1 and PAO1 wbpL, a Strain with a Truncated Lipopolysaccharide. *Appl. Environ. Microbiol.* **2008**, *74*, 6980−6986.
(30) Cho, J.; Choi, H.; Kim, I. S.; Amy, G. Chemical Aspects and by-Products of Electrolyser. *Water Sci. Technol.* **2001**, *1*, 159−167.
(31) Guyot, S.; Ferret, E.; Boehm, J.-B.; Gervais, P. Yeast Cell Inactivation Related to Local Heating Induced by Low-Intensity Electric Fields with Long-Duration Pulses. *Int. J. Food Microbiol.* **2007**, *113*, 180−188.
(32) Zimmermann, U. Electrical Breakdown, Electropermeabilization and Electrofusion. *Rev. Physiol., Biochem. Pharmacol.* **1986**, *105*, 176−256.
(33) Jeong, J.; Kim, J. Y.; Cho, M.; Choi, W.; Yoon, J. Inactivation of Escherichia Coli in the Electrochemical Disinfection Process Using a Pt Anode. *Chemosphere* **2007**, *67*, 652−659.
(34) Van Loey, A.; Verachtert, B.; Hendrickx, M. Effects of High Electric Field Pulses on Enzymes. *Trends Food Sci. Technol.* **2001**, *12*, 94−102.
(35) Aronsson, K.; Lindgren, M.; Johansson, B. R.; Rönner, U. Inactivation of Microorganisms Using Pulsed Electric Fields: The Influence of Process Parameters on Escherichia Coli, Listeria Innocua,

DOI: 10.1021/acsami.7b04863
ACS Appl. Mater. Interfaces 2017, 9, 18238−18247

Leuconostoc Mesenteroides and Saccharomyces Cerevisiae. *Innovative Food Sci. Emerging Technol.* **2001**, *2*, 41−54.
(36) Wardrip, N. C.; Dsouza, M.; Urgun-Demirtas, M.; Snyder, S. W.; Gilbert, J.; Arnusch, C. J. Printing Assisted Modification of Patterned Ultrafiltration Membranes. *ACS Appl. Mater. Interfaces* **2016**, *8*, 30271−30280.
(37) Liu, S.; Hu, M.; Zeng, T. H.; Wu, R.; Jiang, R.; Wei, J.; Wang, L.; Kong, J.; Chen, Y. Lateral Dimension-Dependent Antibacterial Activity of Graphene Oxide Sheets. *Langmuir* **2012**, *28*, 12364−12372.
(38) Herzberg, M.; Elimelech, M. Biofouling of Reverse Osmosis Membranes: Role of Biofilm-Enhanced Osmotic Pressure. *J. Membr. Sci.* **2007**, *295*, 11−20.
(39) Sweity, A.; Zere, T. R.; David, I.; Bason, S.; Oren, Y.; Ronen, Z.; Herzberg, M. Side Effects of Antiscalants on Biofouling of Reverse Osmosis Membranes in Brackish Water Desalination. *J. Membr. Sci.* **2015**, *481*, 172−187.
(40) Givskov, M.; Hentzer, M.; Ersbøll, B. K.; Heydorn, A.; Sternberg, C.; Nielsen, A. T.; Molin, S. Quantification of Biofilm Structures by the Novel Computer Program Comstat. *Microbiology* **2000**, *146*, 2395−2407.

DOI: 10.1021/acsami.7b04863
ACS Appl. Mater. Interfaces 2017, 9, 18238−18247